

# 1      Glacial runoff promotes deep burial of sulfur cycling-associated 2      microorganisms in marine sediments 3

4      Claus Pelikan<sup>1,2</sup>, Marion Jaussi<sup>3</sup>, Kenneth Wasmund<sup>1,2</sup>, Marit-Solveig Seidenkrantz<sup>4</sup>,  
5      Christof Pearce<sup>4</sup>, Zou Zou Anna Kuzyk<sup>5</sup>, Craig W. Herbold<sup>1</sup>, Hans Røy<sup>3</sup>, Kasper Urup  
6      Kjeldsen<sup>3</sup>, and Alexander Loy<sup>1,2\*</sup>

7      <sup>1</sup>Division of Microbial Ecology, Centre for Microbiology and Environmental Systems Science,  
8      University of Vienna, Vienna, Austria

9      <sup>2</sup>Austrian Polar Research Institute, Vienna, Austria

10     <sup>3</sup>Center for Geomicrobiology and Section for Microbiology, Department of Bioscience, Aarhus  
11     University, Aarhus, Denmark

12     <sup>4</sup>Department of Geoscience, iClimate, and Arctic Research Centre, Aarhus University, Denmark

13     <sup>5</sup>Department of Geological Sciences, University of Manitoba, Winnipeg, Canada

14     **\*Correspondence:**

15     Alexander Loy (Tel: +43 1 4277 91205, [loy@microbial-ecology.net](mailto:loy@microbial-ecology.net))

16     **Running Head:** Glacial runoff impacts benthic microbiota

17     **Keywords:** sulfate-reducing microorganisms, marine sediment, glacial impact, deep biosphere,  
18     microbial community assembly, Greenland, arctic

19     5584 words, 2 tables, and 5 figures

## 20     **Contribution to the Field Statement**

21     In most coastal marine sediments organic matter turnover and total energy flux are highest at the  
22     surface and decrease significantly with increasing sediment depth, causing depth-dependent  
23     changes in the microbial community composition. Glacial runoff in arctic and subarctic fjords  
24     alters the composition of the microbial community at the surface, mainly due to different  
25     availabilities of organic matter and metals. Here we show that glacial runoff also modifies  
26     microbial community assembly with sediment depth. Sediment age was a key driver of microbial  
27     community composition in six-meter-long marine sediment cores from the Godthåbsfjord region,  
28     south-western Greenland. High sedimentation rates at glacier-influenced sediment stations  
29     enabled a complex community of sulfur-cycling-associated microorganisms to continuously  
30     thrive at high relative abundances from the surface into the sediment subsurface. These  
31     communities consisted of putative fermenters, sulfate reducers and sulfur oxidizers, which likely  
32     depended on high metal concentrations in the relatively young, glacier-influenced sediments. In  
33     non-glacier-influenced sediments with lower sedimentation rates, these sulfur-cycling-associated  
34     microorganisms were only present near the surface. With increasing sediment depth these  
35     surface microorganisms were largely replaced by other surface microorganisms that positively  
36     correlated with sediment age and belong to known taxa of the energy-limited, marine deep  
37     biosphere.

38

39

40

41

42

43

44

45

46 **Abstract**

47

48 Marine fjords with active glacier outlets are hot spots for organic matter burial in the sediments  
49 and subsequent microbial mineralization, and will be increasingly important as climate warming  
50 causes more rapid glacial melt. Here, we investigated controls on microbial community assembly  
51 in sub-arctic glacier-influenced (GI) and non-glacier-influenced (NGI) marine sediments in the  
52 Godthåbsfjord region, south-western Greenland. We used a correlative approach integrating 16S  
53 rRNA gene and dissimilatory sulfite reductase (*dsrB*) amplicon sequence data over six meters of  
54 depth with biogeochemistry, sulfur-cycling activities, and sediment ages. GI sediments were  
55 characterized by comparably high sedimentation rates and had 'young' sediment ages of <500  
56 years even at 6 m sediment depth. In contrast, NGI stations reached ages of approximately  
57 10,000 years at these depths. Sediment age-depth relationships, sulfate reduction rates, and C/N  
58 ratios were strongly correlated with differences in microbial community composition between GI  
59 and NGI sediments, indicating that age and diagenetic state were key drivers of microbial  
60 community assembly in subsurface sediments. Similar bacterial and archaeal communities were  
61 present in the surface sediments of all stations, whereas only in GI sediments were many surface  
62 taxa also abundant through the whole sediment core. The relative abundance of these taxa,  
63 including diverse *Desulfobacteraceae* members, correlated positively with sulfate reduction  
64 rates, indicating their active contributions to sulfur-cycling processes. In contrast, other surface  
65 community members, such as *Desulfatiglans*, *Atribacteria* and *Chloroflexi*, survived the slow  
66 sediment burial at NGI stations and dominated in the deepest sediment layers. These taxa are  
67 typical for the energy-limited marine deep biosphere and their relative abundances correlated  
68 positively with sediment age. In conclusion, our data suggests that high rates of sediment  
69 accumulation caused by glacier runoff and associated changes in biogeochemistry, promote  
70 persistence of sulfur-cycling activity and burial of a larger fraction of the surface microbial  
71 community into the deep subsurface.

72

73

74 **Introduction**

75

76 Arctic fjords with marine-terminating glaciers constitute an important interface for freshwater  
77 and sediment influx from land into the sea, thereby influencing the physical and chemical  
78 conditions in the coastal marine ecosystems (Etherington et al., 2007; Svendsen et al., 2002). The  
79 high influx of sedimentary materials, e.g., minerals, terrigenous organic matter and metals, in  
80 glacier-associated fjords has a strong effect on the distributions of the benthic microbial  
81 communities (Bourgeois et al., 2016; Buongiorno et al., 2019; Park et al., 2011). Increased water  
82 turbidity in close proximity to the glacier can negatively influence surface water primary  
83 production (Etherington et al., 2007; Zajączkowski, 2008), which leads to lower organic matter  
84 availability in the underlying sediments (Bourgeois et al., 2016). High sediment accumulation  
85 rates often seen in such glacier-proximal environments are also limiting benthic life. On the other  
86 hand, glacial meltwater also provides an important source of dissolved nutrients, which can  
87 stimulate phytoplankton growth beyond the high turbidity zone (Meire et al., 2015; Sørensen et  
88 al., 2015; Statham et al., 2008). Consequences of increased primary production together with  
89 strong sediment supply are a net CO<sub>2</sub> uptake in glaciated fjords as well as rapid burial of fresh  
90 detrital phytoplankton biomass to the underlying sediments (Bourgeois et al., 2016; Meire et al.,  
91 2015; Smith et al., 2015). Fjord sediments also receive significant amounts of terrigenous

92 organic matter as evidenced by high C/N ratios of the sediment organic matter pool (Goñi et al.,  
93 2013; Wehrmann et al., 2014). With these large inputs of both marine and terrigenous organic  
94 matter, the ultimate role of glaciated fjord sediments in the global carbon cycle depends on the  
95 extent to which the large organic matter inputs get degraded, and thus there is a need to better  
96 understand constraints on microbial community structure and degradation potential.

97 The labile fraction of organic matter in marine sediments is initially degraded by  
98 microorganisms with hydrolytic and fermenting capabilities (Müller et al., 2018). These largely  
99 unidentified microbial species typically excrete a wide range of enzymes, which enable rapid  
100 organic matter turnover even in cold arctic sediments (Arnoldi et al., 1998; Teske et al., 2011).  
101 Fermentation products released by primary organic matter degrading microorganisms are either  
102 further degraded by secondary fermenters or are mineralized completely to CO<sub>2</sub> via microbial  
103 respiration (Arndt et al., 2013).

104 Of prime importance in microbial organic matter degradation is the respiratory reduction  
105 of sulfate to sulfide, which facilitates up to 69% of the total organic matter mineralization in  
106 Arctic fjord sediments (Sørensen et al., 2015). Other key electron acceptors are metals such as  
107 iron(oxyhydr)oxides and manganese oxides that can be introduced in high amounts via glacial  
108 runoff to marine sediments and are subjected to redox cycling (Bhatia et al., 2013; Buongiorno et  
109 al., 2019; Laufer et al., 2016; Wehrmann et al., 2014). Fe(III) and Mn(IV) also facilitate the  
110 oxidation of reduced sulfur compounds (Wehrmann et al., 2014; Zopfi et al., 2004) and thereby  
111 fuel a cryptic sulfur cycle in glacier-influenced sediments (Wehrmann et al., 2017).

112 In sediments with comparably slow sediment accumulation, which typify non-glaciated  
113 Arctic shelf areas (Kuzyk et al., 2013), the rate of organic matter mineralization is highest at the  
114 surface and decreases significantly with increasing sediment depth (Kuzyk et al., 2017; Lomstein  
115 et al., 2012), reflecting a concomitant decrease in energy available for cell maintenance and  
116 growth (Starnawski et al., 2017). This depth gradient results in pronounced compositional  
117 changes in the benthic microbial community, which are driven by highly selective survival of  
118 microorganisms that are able to subsist in the energy-limited subsurface (Bird et al., 2019;  
119 Marshall et al., 2019; Petro et al., 2017; Starnawski et al., 2017). Here, we hypothesized that this  
120 strong environmental filtering effect would be attenuated in sediments with high rates of  
121 sedimentation (i.e., in coastal sediments impacted by glacial runoff) and result in a different  
122 pattern of microbial community assembly with depth. Therefore, we investigated microbial  
123 diversity and community compositions of glacier-influenced (GI) and non-glacier-influenced  
124 (NGI) coastal sediments in the Godthåbsfjord region of Greenland. Compositions of bacterial  
125 and archaeal communities and the community of putative sulfite/sulfate-reducing  
126 microorganisms (SRM), as analyzed by 16S rRNA and dissimilatory sulfite reductase (*dsrB*)  
127 gene amplicon sequencing, respectively, were compared across sediment samples of different  
128 depths and ages. Co-occurrence analyses of operational taxonomic units (OTUs) and correlations  
129 with biogeochemical data revealed key environmental factors that were driving the major  
130 community differences between GI and NGI sediments. These analyses also identified various  
131 uncultivated microorganisms that were associated with sulfur cycling. As hypothesized, our  
132 results demonstrate that glacial runoff exerts a strong influence on microbial community  
133 assembly processes and community functions in marine sediments.

134

## 135 Materials and Methods

136

### 137 *Sediment sampling*

138 The sediment cores used in this study were collected using a gravity corer in 2013 during a  
139 research cruise on board of RV *Sanna* (Seidenkrantz et al., 2014). Sampling of the cores for this  
140 study was described previously (Glombitza et al., 2015). In brief, up to 6 m long gravity cores  
141 were recovered from four sites on the open shelf and within the Godthåbsfjord (Nuup Kangerlua)  
142 system in South West Greenland (Table 1, Supplementary Figure S1) in August 2013. The four  
143 stations can be broadly subdivided into two groups. First, the non-glacier-influenced (NGI)  
144 stations 3 and 6. Station 3 (core SA13-ST3-20G) is located outside the fjord on the continental  
145 shelf of the Labrador Sea. Station 6 (core SA13-ST6-40G) is situated in the Kapisigdit  
146 Kanderdluat, a side-fjord without glaciers. Second, the glacier-influenced (GI) stations 5 and 8.  
147 Station 5 (core SA13-ST5-30G) is located in the main channel of the Godthåbsfjord. Although  
148 station 5 is not directly in front of a glacier, most glacier-derived material is transported towards  
149 the Labrador Sea across this site. Station 8 (core SA13-ST8-47G) is in very close proximity to a  
150 glacier front at the northernmost outlet of the Greenland ice sheet in the Kangersuneq fjord  
151 (Supplementary Figure S1).

152 For molecular analyses, sediment cores were sampled by cutting small holes into the core  
153 liner and scraping off the surface with sterile spatulas before collecting sediment samples in  
154 duplicates with sterile 5 mL cut-off syringes. The sediment sub-samples were packed in Whirl-  
155 Pak bags and immediately frozen at -80°C. Porewater was extracted from the sediment cores as  
156 described previously (Glombitza et al., 2015).

157

#### 158 *Analytical methods*

159 Sulfate, hydrogen sulfide, and dissolved inorganic carbon (DIC) concentration measurements, as  
160 well as sulfate reduction rate (SRR) measurements were previously described in Glombitza et al.  
161 (2015). In addition, ferrous iron, total organic carbon (TOC), and total nitrogen (TN) were  
162 analyzed. For analyses of ferrous iron ( $Fe^{2+}$ ) concentrations, porewater was amended with 0.5 M  
163 HCl (1:1, v/v) and stored at 4°C. One mL of ferrozine solution (1 g  $L^{-1}$  in 50 mM HEPES-buffer  
164 at pH 7) was subsequently added to 20  $\mu$ L of acid-preserved porewater, producing a magenta  
165 color reaction (Phillips and Lovley, 1987; Sørensen, 1982). The absorbance was measured at 562  
166 nm (Stookey, 1970) with a spectrophotometer (FLUOstar Omega, BMG Labtech GMBH). To  
167 determine total organic carbon (TOC) and total nitrogen (TN), sediment samples were treated  
168 with sulfuric acid (5-6% w/w) to remove inorganic carbon. Once dried, 50 mg of acidified  
169 sediment were packed into cleaned tin cups and burned in the elemental analyzer (FLASH EA  
170 1112 series, Thermo Scientific). TOC and TN concentrations were calculated from a standard  
171 curve with wheat flour, which contains 43.37% of carbon and 2.31% of nitrogen. The C/N ratio  
172 was calculated as the molar ratio of total organic carbon to total nitrogen. For determination of  
173 methane concentrations, 2  $cm^3$  sediment was transferred to 20 mL GC vials containing 2.5 mL  
174 saturated NaCl with excess crystalline salt. The bottles were vigorously shaken to release  
175 methane into the headspace of the GC vials and stored upside down at -20°C until further  
176 analysis. Methane concentrations in the vial headspace were subsequently measured by gas  
177 chromatography (SRI 310C GC, SRI Instruments Europe GmbH) with a flame ionization  
178 detector. Ammonium concentrations were determined from 2 mL of porewater. Concentrations  
179 were analyzed spectrophotometrically as previously described (Dansk-Standard, 1975) (Bower  
180 and Holm-Hansen, 1980).

181 Sediment age profiles for cores from stations 3, 5, and 6 were based on radiocarbon  
182 dating and age modeling. Materials and depths were chosen for dating based on availability. For  
183 the  $^{14}C$  age determination, calcareous mollusk shells, benthic foraminifera, and seaweed samples

184 were collected from cores and the  $^{14}\text{C}$  concentrations were determined by Accelerator Mass  
185 Spectrometry at the AMS  $^{14}\text{C}$  Dating Centre of Aarhus University. The  $^{14}\text{C}$  ages were calibrated  
186 using the Marine13 radiocarbon calibration curve (Reimer et al., 2013) with a reservoir  
187 correction of  $\Delta\text{R} = 140 \pm 35$  years. Age-depth models for cores from station 3 and 6 were  
188 calculated using the software Oxcal v4.2 (Ramsey, 2008). The presence of rapidly deposited  
189 turbidite sequences in the core from station 5 made a detailed age model difficult.

190 In the core retrieved from station 8 no material usable for  $^{14}\text{C}$  dating was found, and thus  
191 radiocarbon dating was not possible. Instead, the sediment age was estimated from  $^{210}\text{Pb}$  and  
192  $^{226}\text{Ra}$  measurements of freeze-dried, homogenized sediment samples. The water content of each  
193 sample was determined before and after freeze-drying, and results were reported on a dry-weight  
194 basis and salt-corrected for bottom-water salinity at the time of sampling. Core sections were  
195 analyzed by gamma spectroscopy using a CANBERRA® Broad Energy Germanium with a P-  
196 type detector (model BE3830). Detector efficiency and self-absorption were corrected by  
197 counting reference material from the International Atomic Energy Agency (IAEA) within the  
198 same geometry. The reproducibility errors, determined by counting the same sample four times,  
199 were 5.7 and 3.8%, for  $^{210}\text{Pb}$  and  $^{226}\text{Ra}$ , respectively.  $^{210}\text{Pb}$  was also determined from its  $^{210}\text{Po}$   
200 daughter isotope using alpha spectroscopy ( $n=23$  sediment sections). The samples were prepared  
201 as previously described (Flynn, 1968). A  $^{209}\text{Po}$  tracer, calibrated against a  $^{210}\text{Po}$  NIST standard  
202 (Isotope Product Laboratories) was employed for quantitation. The reproducibility error was less  
203 than 1%. Sedimentation rates that were used for the age model presented in this study were  
204 estimated from the least-squares fit to the natural log of the excess  $^{210}\text{Pb}$  ( $^{210}\text{Pbex}$ ) in the core and  
205 the output of a one-dimensional two-layer advection diffusion model that accounts for both  
206 bioturbation and compaction with depth (Kuzyk et al., 2015; Lavelle et al., 1985). When using  
207 any tracer data for age model reconstructions within marine sediments, it is important to  
208 recognize that profiles may be affected by mixing (physical or bioturbation). Physical  
209 disturbance such as a rapid deposition event (turbidite) may be seen in, for example, reversal in  
210 the sediment porosity gradient and unusually low  $^{210}\text{Pb}$  profiles in a particular layer. Many  
211 organic-rich shelf sediment cores exhibit two-layer  $^{210}\text{Pb}$  profiles reflecting a ‘surface mixed  
212 layer’ (SML) overlying accumulating sediments that are subject to little or no mixing (Kuzyk et  
213 al., 2013). If mixing rates are significant relative to sediment accumulation, then it is not possible  
214 to assign ages to specific sediment sections because each section will contain a distribution of  
215 various ages. In the case of station 8, the sediments are low in organics and  $^{210}\text{Pbex}$  decreases  
216 exponentially with depth, implying that mixing is minor relative to sediment accumulation.  
217 Furthermore, the sediment is highly laminated, indicating very little mixing.

218  
219 To estimate the loss of surface sediment by gravity coring and to correct the age-depth  
220 model, we compared the porewater profiles of ammonium, dissolved inorganic carbon and the  
221 carbon isotope ratio  $^{13}\text{C}/^{12}\text{C}$  of DIC (data not shown) between Rumohr cores collected during the  
222 same cruise and the gravity cores presented in this study. The upper 18 cm of the gravity core  
223 retrieved at station 3 and the upper 10 cm of the core retrieved at station 6 were missing. The  
224 depths of potential surface sediment loss at the two GI stations were corrected as the mean values  
225 of the two first cores (14 cm) since the Rumohr core casts at the GI stations were not successful.  
226 Finally, sediment age was recalculated as “actual age”, i.e., the surface of the seafloor was  
227 considered as 0 year old at the time of sampling, based on the age models and the above  
228 mentioned depth correction.

229

230 *DNA extraction and preparation of 16S rRNA gene and dsrB amplicon libraries*

231 Approximately 0.5 to 1 g of sediment was used for DNA extraction according to a previously  
232 established protocol (Kjeldsen et al., 2007). Per station, 8 to 10 samples from different depths,  
233 corresponding to approximately 2 samples per meter core were selected for further analyses, with  
234 highest resolution at the top of the cores (Supplementary Table S1). Barcoded 16S rRNA gene  
235 amplicons were produced with a two-step PCR barcoding approach (Herbold et al., 2015), using  
236 the general bacterial and archaeal primers U519F (5'-CAGCMGCCGCGTAATWC-3') and  
237 802R (5'-TACNVGGGTATCTAATCC-3') for initial amplification (Klindworth et al., 2013).  
238 These primers were modified with a 16 bp head sequence as described previously (Herbold et al.,  
239 2015). The first round of amplification was performed in triplicates with 12.5 µL per reaction  
240 volume. The reaction mix contained 1× Taq buffer (Thermo Scientific), 0.2 mM dNTP mix  
241 (Thermo Scientific), 2 mM MgCl<sub>2</sub>, 0.25 U Taq polymerase (Thermo Scientific), 0.2 µM of each  
242 primer and approximately 1-10 ng DNA. The PCR started with a denaturation at 95°C for 3 min,  
243 followed by 30 cycles of 95°C for 30 s, 48°C for 30 s and 72°C for 30 s, and a final elongation at  
244 72°C for 2 min. The subsequent barcoding PCR round (50 µL total volume) was performed with  
245 1× Taq buffer (Thermo Scientific), 0.2 mM dNTP mix (Thermo Scientific), 2 mM MgCl<sub>2</sub>, 1 U  
246 Taq polymerase (Thermo Scientific), 0.2 µM of each primer and 2 µL of the pooled triplicate  
247 PCR products from the first PCR reaction. The thermal cycling program consisted of an initial  
248 denaturation at 95°C for 3 min, 12 cycles of 95°C for 30 s, 52°C for 30 s and 72°C for 30 s,  
249 followed by a final elongation at 72°C for 2 min. The *dsrB* amplicons were produced according  
250 to an established protocol (Pelikan et al., 2016). Barcoded amplicons were mixed and further  
251 prepared for multiplexed, paired-end MiSeq sequencing (Herbold et al., 2015). Sequence data-  
252 sets are available in the NCBI Sequence Read Archive under study accession number  
253 PRJNA546002.

254

255 *Sequence data processing*

256 16S rRNA gene and *dsrB* amplicon raw reads were demultiplexed, filtered and clustered as  
257 described previously (Herbold et al., 2015; Pelikan et al., 2016) using fastq-join (Aronesty, 2013)  
258 to merge reads and UPARSE version 8.1.1861 (Edgar, 2013) to generate OTUs. Phylum/class-  
259 level classification of 16S rRNA-OTUs was performed with the Ribosomal Database Project  
260 naïve Bayesian classifier in MOTHUR (Schloss et al., 2009; Wang et al., 2007), using the  
261 SILVA database v.128 (Quast et al., 2013) as a reference. *dsrB*-OTUs were classified by  
262 phylogenetic placement of representative sequences into a DsrAB reference tree (Müller et al.,  
263 2015) that was updated with novel sequences from diverse candidate phyla (Anantharaman et al.,  
264 2017; Hausmann et al., 2018; Parks et al., 2017). This DsrAB reference tree was constructed by  
265 de-replicating novel DsrA and DsrB sequences with less than 100 % similarity to any DsrAB  
266 sequence in the original reference database and aligning them to the reference alignments of  
267 DsrA and DsrB (Müller et al., 2015) using MAFFT (Katoh et al., 2002). The combined DsrA and  
268 DsrB alignments were then concatenated and sequences with a total length of less than 500  
269 amino acids were removed. The concatenated DsrAB alignment was clustered at 70 % sequence  
270 identity with usearch (Edgar, 2010), and alignment positions were kept if they were conserved in  
271 at least 10 % of all sequences in the 70%-clustered alignment (56 sequences). The unclustered  
272 DsrAB alignment (2985 sequences) was then filtered for conserved alignment positions using  
273 seqmagick (<https://fhcrc.github.io/seqmagick/>) and was used to generate a maximum likelihood  
274 tree with FastTree (Price et al., 2010). 16S rRNA gene and *dsrB* OTU tables were processed in R  
275 using native functions (R Core Team, 2015) and the R software package phyloseq (McMurdie

276 and Holmes, 2013). OTU counts were rarefied, i.e., sub-sampled at the smallest library size  
277 (*dsrB*: 1521; 16S rRNA gene: 4517) and transformed into relative abundances for all further  
278 analyses, except for network analyses, which were performed with the unrarefied OTU count  
279 matrices (Friedman and Alm, 2012).

280

### 281 *Statistical analyses*

282 Shannon alpha diversity was calculated using R (R Core Team, 2015). Beta diversity analyses  
283 were performed with the R software package vegan (Oksanen et al., 2017), including  
284 calculations of Bray-Curtis distances with the function ‘vegdist()’ and nonmetric  
285 multidimensional scaling ordination analysis with the function ‘nMDS()’. Environmental  
286 variables were tested for effects on the overall community composition by Mantel tests using the  
287 native R function ‘mantel()’. Obtained p-values were corrected for multiple testing with the  
288 native R function ‘p-adjust()’ using the Benjamini-Hochberg correction method. Correlations of  
289 individual OTUs with environmental variables were calculated with the native R function cor()  
290 using the Spearman correlation coefficient. P-values were generated by permuting the values of  
291 each environmental variable followed by correlation of individual OTU abundances with the  
292 permuted environmental variable. This process was repeated 1000 times and the obtained p-  
293 values were corrected as described above.

294 Correlation network analyses were performed separately for 16S rRNA- and *dsrB*-OTUs  
295 to highlight potential synergistic interactions between microbial community members (Weiss et  
296 al., 2016). Species co-occurrence networks were calculated using SparCC (Friedman and Alm,  
297 2012) based on count matrices of all OTUs with >10 reads in at least 7 out of 34 samples. Use of  
298 more abundant and prevalent OTUs increases sensitivity of the network analyses (Berry and  
299 Widder, 2014). P-values were generated as described above. Only positive OTU correlations  
300 >0.5 were considered. Attributes of individual OTUs, i.e., sampling station and sediment age at  
301 which the OTU was found at the highest relative abundance, were assigned to OTUs in R and  
302 networks were visualized in Cytoscape (Shannon et al., 2003). Significant OTU clusters, i.e.,  
303 significantly more interactions between OTUs within the community cluster than with OTUs  
304 outside the community cluster, were defined by Mann-Whitney U tests using the Cytoscape  
305 plugin “clusterONE” (Nepusz et al., 2012).

306

### 307 *Phylogenetic analysis*

308 Representative sequences of 16S rRNA-OTUs were aligned with the SINA aligner (Pruesse et  
309 al., 2012) using the SILVA database v.128 (Quast et al., 2013) as a reference. Sequences that  
310 were closely related to 16S rRNA-OTUs were extracted from the SILVA database and used to  
311 construct a reference tree with FastTree (Price et al., 2010). Subsequently, 16S rRNA-OTU  
312 sequences were placed into the reference tree using the EPA algorithm (Berger et al., 2011) in  
313 RAxML (Stamatakis, 2014). The placement trees of 16S rRNA-OTUs and *dsrB*-OTUs (utilized  
314 for *dsrB*-OTU classification) were visualized with iTOL (Letunic and Bork, 2007).

315

316

## 317 **Results**

318

319 *Depth profiles of sediment age and porewater chemistry differ substantially between non-*  
320 *glacier-influenced and glacier-influenced sediments*

321 A goal of the present study was to identify environmental factors (biogeochemical data is  
322 partially described in Glombitza *et al.*, 2015) that shape the microbial community compositions  
323 and interactions in NGI and GI sediments. NGI stations 3 and 6 are located on the open shelf and  
324 within the Godthåbsfjord, respectively, and were both characterized by a strong gradient of  
325 sediment age due to comparably low sedimentation rates with maximum ages of the gravity  
326 cores close to 10,000 years (Figure 1). Furthermore, NGI sediments had high TOC and TN  
327 concentrations, as well as low C/N ratios down to 500 cm sediment depth. SRR decreased with  
328 depth at both stations and sulfate became depleted in the bottom of the core from station 3, but  
329 not in the core from station 6. At station 3, hydrogen sulfide concentrations gradually increased  
330 with depth and decreased again below a depth of 400 cmbsf, coinciding with the appearance of  
331 methane in the porewater. At station 6, hydrogen sulfide was present in lower amounts and  
332 methane did not accumulate at any depth.

333 In comparison, GI stations 5 and 8 were both characterized by high sedimentation rates as  
334 indicated by the low sediment ages, i.e., around 200 years at the bottom of the core at station 8  
335 and around 500 years at the bottom of the core at station 5 (Figure 1). GI stations had low TOC  
336 and TN concentrations, as well as high C/N ratios of up to 48. The porewater contained dissolved  
337  $\text{Fe}^{2+}$  in the upper 250 cmbsf at both GI stations. SRR were high in deeper sediment layers at the  
338 GI stations. Notably, SRR in the deep sediments of station 8 were higher than those measured in  
339 the uppermost sediment samples from the core retrieved at station 3. Despite substantial SRR,  
340 hydrogen sulfide was not detected at any depth.

341  
342 *Glacier runoff and sediment age are strong determinants of microbial community composition*  
343 In total, 6755 16S rRNA-OTUs and 1094 *dsrB*-OTUs were obtained by amplicon sequencing.  
344 NGI and GI sediments clearly differed in 16S rRNA- and *dsrB*-OTU compositions and these  
345 differences increased with depth at NGI stations (Supplementary Figure S2 A and B). Mantel  
346 correlations with environmental factors revealed that the 16S rRNA- and *dsrB*-OTU  
347 compositions were mostly impacted by sediment age and C/N ratio of organic matter (Table 2).  
348 Further differences in 16S rRNA gene and *dsrB*-OTU compositions were explained to a lesser  
349 extent by sediment structure (i.e., density and porosity), TOC, TN, SRR and  $\text{Fe}^{2+}$  concentrations  
350 (the latter two parameters were only significant for the 16S rRNA gene community) (Table 2).  
351 Gradually increasing sediment age with depth at NGI stations (Figure 1) was associated with  
352 gradual changes in 16S rRNA gene and *dsrB* beta-diversity with depth (Supplementary Figure  
353 S2 A and B). 16S rRNA and *dsrB* alpha-diversity at the NGI stations gradually decreased with  
354 depth (Supplementary Figure S2 C and D). In contrast, alpha-diversity in GI stations remained  
355 rather high throughout the cores (Supplementary Figure S2 C and D). Relative abundance  
356 patterns of most phyla/classes and DsrAB families at GI stations 5 and 8 did not follow a gradual  
357 change in compositions with increasing sediment depth like at NGI stations 3 and 6, but  
358 remained rather constant, with some fluctuations among taxa (Figure 2). *Alpha*-, *Delta*- and  
359 *Gammaproteobacteria*, *Campylobacterota* and notably *Cyanobacteria* were overall more  
360 abundant at GI sediments as compared to NGI sediments (Figure 2 A). Furthermore, the *dsrAB*-  
361 containing community in GI sediments had higher relative abundances of *Desulfobacteraceae*,  
362 *Desulfobulbaceae*, uncultured DsrAB family-level lineages 4, 7, and 9 and unclassified DsrAB  
363 sequences from the *Firmicutes* group and the *Nitrospira* supercluster (Figure 2 B). At NGI  
364 stations, several phyla/classes, i.e., *Acidobacteria*, *Bacteroidetes*, *Deltaproteobacteria*,  
365 *Dependentiae* (TM6), *Gammaproteobacteria*, *Omnitrophica* (OP3), *Planctomycetes*, and  
366 *Woesarchaeota* (DHVEG-6) decreased in relative abundance with depth, particularly at station 3

367 (Figure 2 A). The phyla *Atribacter* (JS1), *Aerophobetes* (BHI80–139), *Aminicenantes* (OP8),  
368 *Alphaproteobacteria*, *Betaproteobacteria*, and *Chloroflexi* increased in relative 16S rRNA gene  
369 abundances with depth at both NGI stations (Figure 2 A). The relative abundances of the  
370 following *dsrAB*-containing groups decreased with depth at NGI stations: *Desulfobacteraceae*,  
371 *Syntrophobacteraceae*, the uncultured family-level lineages 7 and 9, and uncultured bacteria  
372 within the Environmental supercluster 1 (Figure 2 B). In contrast, representatives of the  
373 uncultured family-level lineage 3, as well as uncultured bacteria within the *Delta*  
374 *proteobacteria* supercluster and the *Firmicutes* group, increased in relative abundances with depth at the NGI  
375 stations.

376  
377 *OTUs that were positively correlated to SRR have high inter-species connectivity in young*  
378 *sediments*

379 Correlation network analyses of 16S rRNA- and *dsrB*-OTUs revealed two nearly separated 16S  
380 rRNA-OTU clusters and two completely separated *dsrB*-OTU clusters, which were structured  
381 along a sediment age gradient (Figure 3 A and B). One cluster included OTUs that were most  
382 abundant in old NGI sediments and the other one included OTUs that were most abundant in  
383 young GI and NGI sediments. These separate network clusters in ‘young’ and ‘old’ sediments  
384 largely overlapped with regions of particularly high inter-species OTU correlations. These  
385 ‘young’ and ‘old’ sediment OTU clusters were separated at a sediment age of around 300–400  
386 years (Figure 3 C and D), which corresponds to a sediment depth of 30–40 and 20–30 cmbsf at  
387 NGI stations 3 and 6, respectively.

388 The OTUs in the 16S rRNA- and *dsrB*-OTU networks were additionally subjected to  
389 correlation analyses with environmental parameters (Supplementary Figures S3 and S4). The  
390 majority of OTUs that constituted the ‘young’ and ‘old’ sediment clusters were positively  
391 correlated with SRR and sediment age, respectively (Figure 3 A and B). Most OTUs that  
392 correlated positively with SRR also correlated negatively with sediment age and vice versa  
393 (Supplementary Figures S3 and S4). OTUs that positively correlated to SRR showed distinct  
394 distributions in relative abundances, i.e., highest abundances in the surface sediments of NGI  
395 stations and mostly ubiquitous distributions throughout the whole core at GI stations (Figure 4).  
396 Many of these 16S rRNA-OTUs ( $n=10$ ) and most of the *dsrB*-OTUs belonged to the family  
397 *Desulfobacteraceae* (Supplementary Figures S5 and S6). Other SRR-correlated 16S rRNA-  
398 OTUs belonged to the families *Desulfobulbaceae*, *Desulfarculaceae*, and *Syntrophobacteraceae*  
399 and to the phyla/classes, *Acidobacteria*, *Actinobacteria*, *Alphaproteobacteria*, *Bacteroidetes*,  
400 *Ignavibacteria*, *Gammaproteobacteria*, *Planctomycetes* and *Woesarchaeota* (Supplementary  
401 Figure S5). Besides the prevalence of *Desulfobacteraceae*, *dsrB*-OTUs positively correlated to  
402 SRR were affiliated with the uncultured family-level lineages 7 and 9 (Supplementary Figure  
403 S6). The *dsrB*-OTUs 40 and 41 were also affiliated with the Environmental Supercluster 1. OTU  
404 40 belongs to a sequence cluster of uncultured bacteria, and is related to the metagenome-derived  
405 genome RBG\_13\_60\_13 (accession number GCA\_001796685.1) of a *Chloroflexi* bacterium  
406 (Supplementary Figure S6).

407 OTUs positively correlated with sediment age were affiliated with diverse taxa (Figure  
408 5). The phyla/classes that were represented by at least two age-correlated 16S rRNA-OTUs were  
409 *Aerophobetes* (BHI80–13), *Alphaproteobacteria*, *Aminicenantes* (OP8), *Atribacter* (JS1),  
410 *Chloroflexi*, *Delta*  
411 *proteobacteria*, *Euryarchaeota* (Marine Benthic Group D), *Omnitrophica*  
412 (OP3) and *Planctomycetes* (Supplementary Figure S5). Three *dsrB*-OTUs that positively  
correlated with sediment age were affiliated to the family *Desulfobacteraceae* (Supplementary

413 **Figure S6).** The *dsrB*-OTU 16 belonged to a group of uncultured bacteria in the  
414 *Delta proteobacteria* supercluster, OTU 58 could only be assigned to the *Firmicutes* group, and  
415 OTU 1 was affiliated with the family *Syntrophobacteraceae*.

416

## 417 Discussion

418

419 *Glacier-runoff affects age-depth relationships and microbial community assembly in marine*  
420 *sediments*

421 Rates and amounts of glacial inputs into sedimentary environments of fjords have a major impact  
422 on their biogeochemistry (Glombitza et al., 2015). Here, we have compared microbial  
423 community structure between NGI and GI sediments, and highlighted the environmental factors  
424 that underlie the observed differences in community assembly with sediment depth. Sulfate is the  
425 key terminal electron acceptor in marine sediments of the Godthåbsfjord (Sørensen et al., 2015),  
426 but the depth distributions of SRR and microbial community structures differed between NGI  
427 and GI sediments.

428 In the NGI sediments, steep gradients of SRR (Figure 1) indicated that most of the labile  
429 organic matter deposited from marine primary production was mineralized near the seafloor  
430 surface as typically observed for marine shelf sediments (Flury et al., 2016). Microbial  
431 communities in the NGI sediments became less diverse with depth and increasingly distinct from  
432 the surface communities (Supplementary Figure S2). Such shifts in community composition with  
433 depth can be attributed to the progressing geochemical stratification of the sediment and  
434 decreasing flux of energy with increasing sediment age (Petro et al., 2017).

435 In contrast, the two GI sediment cores were characterized by higher sedimentation rates,  
436 low porosity (station 8), young ages, low TOC concentrations, low TN, and high C/N ratios  
437 (Figure 1); the latter being attributed to influx of terrestrial organic matter (Goñi et al., 2013;  
438 Meyers, 1994; Wehrmann et al., 2014). Terrestrial organic matter of particulate phase  
439 transported by the glaciers is mostly old, diagenetically altered, and likely unavailable for  
440 microbial degradation (Wehrmann et al., 2014). Therefore, the strong impact of C/N ratio  
441 differences on the microbial community might only reflect the high rate of sedimentation. The on  
442 average higher SRR throughout the GI sediment cores were possibly sustained by low amounts  
443 of reactive organic matter that was deposited from algal blooms in nutrient-rich waters of  
444 glaciated fjords (Bourgeois et al., 2016). Glacial runoff also contains considerable amounts of  
445 iron and manganese (Bhatia et al., 2013; Wehrmann et al., 2014). Accumulation of dissolved  
446 Fe<sup>2+</sup> suggested that Fe(III) reduction substantially contributed to organic matter mineralization in  
447 upper GI station sediments (Wehrmann et al., 2014). Lack of sulfide accumulation with depth  
448 indicated immediate re-oxidation and/or scavenging of sulfide produced from high sulfate  
449 reduction activity (Figure 1) (Wehrmann et al., 2017). In agreement with previous studies  
450 (Bourgeois et al., 2016; Buongiorno et al., 2019; Park et al., 2011), differences in organic matter  
451 availability and electron acceptor concentrations are suggested to had a major influence on the  
452 composition of the seafloor microbial community in glaciated fjords.

453

454 *Identities and potential functional interactions of sulfur cycling-associated taxa in 'young' NGI*  
455 *and GI sediments*

456 16S rRNA gene and *dsrB* correlation network analyses both revealed two main OTU interaction  
457 clusters (Figure 3). In one cluster most OTUs were positively correlated to SRR but not sediment  
458 age, while in the other cluster most OTUs were positively correlated to sediment age but not

459 SRR. The relative abundances of 16S rRNA- and *dsrB*-OTUs that positively correlated with SRR  
460 were highest in ‘young’ GI and NGI sediments with active sulfur cycling (up to about 400 years  
461 of age). The majority of these OTUs was affiliated with the family *Desulfobacteraceae*, as well  
462 as other *bona fide* delta- proteobacterial SRM taxa from marine sediments (Wasmund et al., 2017).  
463 In addition, several SRR-correlated *dsrB*-OTUs were affiliated with uncultured DsrAB lineages.  
464 Some of these lineages contain metagenome-derived sequences of uncultivated bacteria from the  
465 phyla *Acidobacteria* (DsrAB family-level lineage 9), *Planctomycetes* or *Chloroflexi*  
466 (Anantharaman et al., 2017; Wasmund et al., 2016). Interestingly, several 16S rRNA-OTUs that  
467 positively correlated with SRR were also affiliated with these phyla, supporting their putative  
468 involvement in sulfite/sulfate reduction or sulfur disproportionation in the Godthåbsfjord  
469 sediments.

470 Despite high rates of sulfate reduction, sulfide did not accumulate in the GI sediments  
471 (Figure 1) likely due to its reaction with metals resulting in its oxidation and/or precipitation  
472 (Wehrmann et al., 2014). Several 16S rRNA-OTUs that correlated positively with SRR were  
473 affiliated with taxa containing sulfur-oxidizing microorganisms such as the candidate genus  
474 PHOS-HE36 (phylum *Ignavibacteriae*) (Koenig et al., 2005), the *Woeseiaceae*/JTB255 sediment  
475 group (*Gammaproteobacteria*) (Dyksma et al., 2016; Mußmann et al., 2017), and the  
476 *Rhodobacteriaceae* (*Alphaproteobacteria*) (Lenk et al., 2012; Thrash et al., 2017)  
477 (Supplementary Figure S5). In addition, OTU 30 affiliated with the sulfur-oxidizing genus  
478 *Sulfurovum* was solely responsible for the high relative abundance of *Campylobacterota* at GI  
479 station 5. We hypothesize that high SRR and chemical oxidation of sulfide by metals may  
480 support significant populations of sulfur-oxidizing or sulfur-disproportionating taxa in deep GI  
481 sediments, although future work would be required to substantiate this hypothesis, e.g., detection  
482 of mRNA transcripts for sulfur-dissimilating enzymes.

483 We also identified numerous SRR-correlated OTUs that were affiliated with taxa that are  
484 not known to have sulfur-based energy metabolisms. While these OTUs could indeed represent  
485 unknown sulfur-cycling microorganisms, they may also be degraders of organic matter that fuel  
486 sulfate reduction with fermentation products. For instance, some of these 16S rRNA-OTUs were  
487 affiliated with BD2-2 (phylum *Bacteroidetes*), *Phycisphaera* (phylum *Planctomycetes*) or OM1  
488 (phylum *Actinobacteria*). Representatives of these phyla hydrolyze and ferment organic  
489 polymers in marine sediments and consequently might have trophic associations with SRM  
490 (Baker et al., 2015; Schauer et al., 2011; Trembath-Reichert et al., 2016; Webster et al., 2011).  
491 These associations may therefore explain their cooccurrences with SRM detected here.

492  
493 *Assembly of the deep subsurface microbial biosphere in NGI sediments*  
494 OTU correlation analysis showed that OTU clusters and thus the microbial communities of  
495 young and old sediment zones in NGI sediments became ‘disconnected’ at a sediment age of  
496 about 300-400 years (Figure 3), corresponding to a sediment depth of approximately 30 cmbsf at  
497 NGI stations. This is in line with observations that a considerable shift in microbial community  
498 structures occur in marine sediments below the zone of bioturbation, which was suggested to be  
499 the main site of assembly of the subsurface community (Jochum et al., 2017; Starnawski et al.,  
500 2017). Most OTUs that positively correlated with sediment ages in NGI sediments were  
501 affiliated with lineages known to harbor members that selectively persist from the surface into  
502 deep subsurface sediments, e.g., *Chloroflexi*, *Aerophobetes*, *Atribacter* (JS1), *Aminicenantes*  
503 (OP8), *Alphaproteobacteria* and *Delta- proteobacteria* (Supplementary Figure S5) (Orcutt et al.,  
504 2011; Wang et al., 2016). Members of these taxa, such as the genus *Desulfatiglans* (Jochum et

505 al., 2018), the delta-proteobacterial candidate lineage SEEP-SRB1 (Schreiber et al., 2010) or the  
506 euryarchaeal Marine Benthic Group D (Kaster et al., 2014; Lloyd et al., 2013; Nobu et al., 2016;  
507 Robbins et al., 2016; Wang et al., 2016b; Wasmund et al., 2014) are postulated to have traits  
508 such as fermentation, sulfate reduction or acetogenesis to support the maintenance of basic  
509 cellular functions even under extreme energy-limited conditions in most subsurface sediment  
510 environments (Petro et al., 2017).

511

## 512 **Conclusions**

513

514 Coastal marine ecosystems in arctic and sub-arctic oceans are poised to be increasingly impacted  
515 by melting of glaciers caused by climate change. In this comparative study, we found that  
516 discharge from marine-terminating glaciers had a strong control over the depth-dependent  
517 microbial community assembly in sediments of a sub-arctic fjord. Increasing differences in the  
518 benthic community composition between GI and NGI sites with depth were largely explained by  
519 sediment age. High sedimentation rates at GI stations enabled a complex community of sulfur-  
520 cycling-associated microorganisms, including both putative SRM and sulfide oxidizers, to  
521 continuously thrive at high relative abundances from the surface deep into the subsurface.  
522 Similar communities of sulfur-cycling-associated microorganisms were also present in surface  
523 sediments at NGI stations. However, with increasing depth the surface communities were largely  
524 replaced by microorganisms that positively correlated with sediment age. Lower sedimentation  
525 rates at the NGI sites thus resulted in slow burial and highly selective survival of microorganisms  
526 adapted to the energy-limited subsurface (Petro et al., 2017). In summary, our results suggest that  
527 increased glacier runoff and the associated high sedimentation rates allow processes that are  
528 typically predominant in surface sediments such as sulfide oxidation and associated community  
529 members to be rapidly buried and maintained at high abundances in deep subsurface sediments.

530

## 531 **Conflict of Interest**

532

533 The authors declare that the research was conducted in the absence of any commercial or  
534 financial relationships that could be construed as a potential conflict of interest.

535

## 536 **Author Contributions**

537

538 CIP, HR, KUK, and AL designed the research. CIP generated and analyzed the sequencing data.  
539 MSS, HR, and ChP collected the sediment cores. MJ, HR, and KK obtained the samples and MJ  
540 performed most biogeochemical analyses. KUK performed DNA extractions. MSS, ChP, and  
541 ZAK calculated sediment ages. CIP, KW, and AL wrote the manuscript. All authors revised the  
542 manuscript.

543

## 544 **Funding**

545

546 The cruise was led by Marit-Solveig Seidenkrantz and funded by the Arctic Research Centre,  
547 Aarhus University. This work was financially supported by the Austrian Science Fund (P29426-  
548 B29 to KW; P25111-B22 to AL) and the Danish National Research Foundation (Grant  
549 DNRF104).

550

551

552 **Acknowledgments**

553

554 The authors thank the crew of the R/V Sanna and the scientific party during the 2013 sampling  
555 campaign and Britta Poulsen and Susanne Nielsen for laboratory technical assistance. We  
556 acknowledge the use of imagery from the NASA Worldview application  
557 (<https://worldview.earthdata.nasa.gov>), part of the NASA Earth Observing System Data and  
558 Information System (EOSDIS).

559

560

561 **Tables**

562

563 **Table 1. Description of the sampling stations and cores, including sampling position, water**  
564 **depth and core length.** Table was modified from Glombitza et al., 2015. The exact location of  
565 the sampling stations is indicated in **Supplementary Figure S1**.

Station	Core name	Latitude (N)	Longitude (W)	Waterdepth (m)	Core length (cm)
3	SA13-ST3-20G	6426.7425'	5247.6486'	498.2	587
5	A13-ST5-30G	6425.3479'	5130.6209'	622.4	607
6	SA13-ST6-40G	6429.0604'	5042.3240'	389	562
8	SA13-ST8-47G	6440.7078'	5017.4672'	475.8	569

566

567

568 **Table 2. Mantel correlations between 16S rRNA gene and *dsrB* community compositions**  
569 **and physicochemical parameters.** Only significant values ( $p < 0.05$ ) are shown in the table.  
570 Parameters with the strongest effect on the 16S rRNA gene or *dsrB* community compositions are  
571 indicated in bold.

	16S rRNA gene		<i>dsrB</i>	
	Mantel statistic	p-value	Mantel statistic	p-value
Sediment age [actual years]	<b>0.380</b>	0.003	<b>0.538</b>	0.002
Sulfate [mmol L <sup>-1</sup> ]	0.179	0.016	0.390	0.002
DIC [mmol L <sup>-1</sup> ]	0.108	0.047	0.207	0.010
H <sub>2</sub> S [μmol L <sup>-1</sup> ]	0.227	0.003	0.418	0.002
Fe(II) [μmol L <sup>-1</sup> ]	0.262	0.003	-	-
Density [g cc <sup>-1</sup> ]	0.234	0.003	0.349	0.002
Porosity	0.213	0.003	0.364	0.002
TOC [μmol g dw <sup>-1</sup> ]	0.228	0.005	0.329	0.002
C/N ratio	<b>0.471</b>	0.003	<b>0.478</b>	0.002
SRR [nmol Sulfate cm <sup>-3</sup> d <sup>-1</sup> ]	0.260	0.003	-	-
Methane [μmol L <sup>-1</sup> ]	-	-	0.310	0.002

572 DIC, dissolved inorganic carbon; TOC, total organic carbon; SRR, sulfate reduction rate

573

574

575 **Figure legends**

576

577 **Figure 1. Physicochemical sediment properties in non-glacier-influenced (NGI) and glacier-**  
578 **influenced (GI) sediment cores.** Colours indicate the sampling station. Note that the scales are  
579 different for each physicochemical parameter. Data on SRR and DIC, as well as, sulfate and  
580 sulfide concentrations were taken from Glombitza et al., 2015.

581

582 **Figure 2. Microbial community composition in non-glacier-influenced (NGI) and glacier-**  
583 **influenced (GI) sediment cores.** Changes in 16S rRNA phylum/class (A) and DsrAB-family  
584 (B) relative abundances with sediment depth are shown. Only phyla/classes and DsrAB-families  
585 with a relative abundance greater than 1% are shown. DS, *Deltaproteobacteria* supercluster.  
586 ES1, Environmental supercluster 1. FG, *Firmicutes* group. NS, *Nitrospira* supercluster.

587

588 **Figure 3. Co-occurrence of abundant OTUs across non-glacier-influenced (NGI) and**  
589 **glacier-influenced (GI) sediment cores.** Inter-species correlations are indicated for 16S rRNA  
590 gene (A) and *dsrB* (B) OTUs. Only edges with  $p \leq 0.01$  and  $R^2 \geq 0.5$  are shown. OTUs are  
591 colored and shaped according to the approximated sediment age and sampling station at which  
592 they were found at the highest relative abundance, respectively. The orange and green border  
593 color of OTUs indicates significant correlations to sulfate reduction rates and sediment age,  
594 respectively. OTUs that are connected by black and purple edges formed significant community  
595 clusters in old and young sediments, respectively. C and D, Age of the sediment layer at which  
596 individual OTUs from (A) and (B) were found at the highest relative abundance across all  
597 samples and stations. Each dot represents an OTU. Black and purple background colors indicate  
598 the affiliation to significant community clusters determined for the inter-species correlation  
599 networks, respectively.

600

601 **Figure 4. Relative abundances of 16S rRNA- and *dsrB*-OTUs with significant correlations**  
602 **to sulfate reduction rates in non-glacier-influenced (NGI) and glacier-influenced (GI)**  
603 **sediment cores.** The column annotation indicates the sampling depth in centimeters below  
604 seafloor (cmbsf). The color range from blue to red indicates the relative abundance of OTUs.  
605 Phyla/classes and DsrAB-families that were represented by more than one OTU are indicated in  
606 bold.

607

608 **Figure 5. Relative abundances of 16S rRNA- and *dsrB*-OTUs with significant correlations**  
609 **to sediment age in non-glacier-influenced (NGI) and glacier-influenced (GI) sediment**  
610 **cores.** The column annotation indicates the sampling depth in centimeters below seafloor  
611 (cmbsf). The color range from blue to red indicates the relative abundance of OTUs.  
612 Phyla/classes and DsrAB-families that were represented by more than one OTU are indicated in  
613 bold.

614

615

616 **References**

617 Anantharaman, K., Hausmann, B., Jungbluth, S. P., Kantor, R. S., Lavy, A., Warren, L. A., et al.  
618 (2018). Expanded diversity of microbial groups that shape the dissimilatory sulfur cycle.  
619 *ISME J.* 12, 1715–1728.

620 Arndt, S., Jørgensen, B. B., LaRowe, D. E., Middelburg, J. J., Pancost, R. D., and Regnier, P.  
621 (2013). Quantifying the degradation of organic matter in marine sediments: A review and  
622 synthesis. *Earth-Sci. Rev.* 123, 53–86.

623 Arnosti, C., Jørgensen, B. B., Sagemann, J., and Thamdrup, B. (1998). Temperature dependence  
624 of microbial degradation of organic matter in marine sediments: polysaccharide hydrolysis,  
625 oxygen consumption, and sulfate reduction. *Marine Ecology Progress Series* 165, 59–70.

626 Aronesty, E. (2013). Comparison of Sequencing Utility Programs. *The Open Bioinformatics  
627 Journal* 7, 1–8.

628 Baker, B. J., Lazar, C. S., Teske, A. P., and Dick, G. J. (2015). Genomic resolution of linkages in  
629 carbon, nitrogen, and sulfur cycling among widespread estuary sediment bacteria.  
630 *Microbiome* 3, 14.

631 Berger, S. A., Krompass, D., and Stamatakis, A. (2011). Performance, accuracy, and Web server  
632 for evolutionary placement of short sequence reads under maximum likelihood. *Syst. Biol.*  
633 60, 291–302.

634 Berry, D., and Widder, S. (2014). Deciphering microbial interactions and detecting keystone  
635 species with co-occurrence networks. *Front. Microbiol.* 5, 219.

636 Bhatia, M. P., Kujawinski, E. B., Das, S. B., Breier, C. F., Henderson, P. B., and Charette, M. A.  
637 (2013). Greenland meltwater as a significant and potentially bioavailable source of iron to  
638 the ocean. *Nat. Geosci.* 6, 503–503.

639 Bird, J. T., Tague, E. D., Zinke, L., Schmidt, J. M., Steen, A. D., Reese, B., et al. (2019).  
640 Uncultured Microbial Phyla Suggest Mechanisms for Multi-Thousand-Year Subsistence in  
641 Baltic Sea Sediments. *MBio* 10. doi:10.1128/mBio.02376-18.

642 Bourgeois, S., Kerhervé, P., Calleja, M. L., Many, G., and Morata, N. (2016). Glacier inputs  
643 influence organic matter composition and prokaryotic distribution in a high Arctic fjord  
644 (Kongsfjorden, Svalbard). *J. Mar. Syst.* 164, 112–127.

645 Bower, C. E., and Holm-Hansen, T. (1980). A Salicylate–Hypochlorite Method for Determining  
646 Ammonia in Seawater. *Canadian Journal of Fisheries and Aquatic Sciences* 37, 794–798.

647 Buongiorno, J., Herbert, L. C., Wehrmann, L. M., Michaud, A., Laufer, K., Røy, H., et al.  
648 (2019). Complex microbial communities drive iron and sulfur cycling in Arctic fjord  
649 sediments. *Appl. Environ. Microbiol.* doi:10.1128/AEM.00949-19.

650 Dansk-Standard. (1975) DS 224: Vandundersøgelse. Bestemmelse af ammonium-nitrogen. 6 pp.

651 Dyksma, S., Bischof, K., Fuchs, B. M., Hoffmann, K., Meier, D., Meyerdierks, A., et al. (2016).  
652 Ubiquitous Gammaproteobacteria dominate dark carbon fixation in coastal sediments. *ISME J.* 10, 1939–1953.

653

654 Edgar, R. C. (2010). Search and clustering orders of magnitude faster than BLAST.  
655 *Bioinformatics* 26, 2460–2461.

656 Edgar, R. C. (2013). UPARSE: highly accurate OTU sequences from microbial amplicon reads.  
657 *Nat. Methods* 10, 996–998.

658 Etherington, L. L., Hooge, P. N., Hooge, E. R., and Hill, D. F. (2007). Oceanography of Glacier  
659 Bay, Alaska: Implications for biological patterns in a glacial fjord estuary. *Estuaries Coasts*  
660 30, 927–944.

661 Flury, S., Røy, H., Dale, A. W., Fossing, H., Tóth, Z., Spiess, V., et al. (2016). Controls on  
662 subsurface methane fluxes and shallow gas formation in Baltic Sea sediment (Aarhus Bay,  
663 Denmark). *Geochim. Cosmochim. Acta* 188, 297–309.

664 Flynn, W. W. (1968). The determination of low levels of polonium-210 in environmental  
665 materials. *Anal. Chim. Acta* 43, 221–226.

666 Friedman, J., and Alm, E. J. (2012). Inferring Correlation Networks from Genomic Survey Data.  
667 *PLoS Comput. Biol.* 8, e1002687.

668 Froelich, P. N., Klinkhammer, G. P., Bender, M. L., Luedtke, N. A., Heath, G. R., Cullen, D., et  
669 al. (1979). Early oxidation of organic matter in pelagic sediments of the eastern equatorial  
670 Atlantic: suboxic diagenesis. *Geochim. Cosmochim. Acta* 43, 1075–1090.

671 Glombitza, C., Jaussi, M., Røy, H., Seidenkrantz, M.-S., Lomstein, B. A., and Jørgensen, B. B.  
672 (2015). Formate, acetate, and propionate as substrates for sulfate reduction in sub-arctic  
673 sediments of Southwest Greenland. *Front. Microbiol.* 6, 846.

674 Goñi, M. A., O'Connor, A. E., Kuzyk, Z. Z., Yunker, M. B., Gobeil, C., and Macdonald, R. W.  
675 (2013). Distribution and sources of organic matter in surface marine sediments across the  
676 North American Arctic margin. *J. Geophys. Res. C: Oceans* 118, 4017–4035.

677 Hausmann, B., Pelikan, C., Herbold, C. W., Köstlbacher, S., Albertsen, M., Eichorst, S. A., et al.  
678 (2018). Peatland Acidobacteria with a dissimilatory sulfur metabolism. *ISME J.* 12, 1729–  
679 1742.

680 Herbold, C. W., Pelikan, C., Kuzyk, O., Hausmann, B., Angel, R., Berry, D., et al. (2015). A  
681 flexible and economical barcoding approach for highly multiplexed amplicon sequencing of  
682 diverse target genes. *Front. Microbiol.* 6, 731.

683 Jochum, L. M., Chen, X., Lever, M. A., Loy, A., Jørgensen, B. B., Schramm, A., et al. (2017).  
684 Depth Distribution and Assembly of Sulfate-Reducing Microbial Communities in Marine

685 Sediments of Aarhus Bay. *Appl. Environ. Microbiol.* 83. doi:10.1128/AEM.01547-17.

686 Jochum, L. M., Schreiber, L., Marshall, I. P. G., Jørgensen, B. B., Schramm, A., and Kjeldsen,  
687 K. U. (2018). Single-Cell Genomics Reveals a Diverse Metabolic Potential of Uncultivated  
688 Desulfatiglans-Related Deltaproteobacteria Widely Distributed in Marine Sediment.  
689 *Frontiers in Microbiology* 9. doi:10.3389/fmicb.2018.02038.

690 Kaster, A.-K., Mayer-Blackwell, K., Pasarelli, B., and Spormann, A. M. (2014). Single cell  
691 genomic study of Dehalococcoides species from deep-sea sediments of the Peruvian  
692 Margin. *ISME J.* 8, 1831–1842.

693 Katoh, K., Misawa, K., Kuma, K.-I., and Miyata, T. (2002). MAFFT: a novel method for rapid  
694 multiple sequence alignment based on fast Fourier transform. *Nucleic Acids Res.* 30, 3059–  
695 3066.

696 Kjeldsen, K. U., Loy, A., Jakobsen, T. F., Thomsen, T. R., Wagner, M., and Ingvorsen, K.  
697 (2007). Diversity of sulfate-reducing bacteria from an extreme hypersaline sediment, Great  
698 Salt Lake (Utah). *FEMS Microbiol. Ecol.* 60, 287–298.

699 Klindworth, A., Pruesse, E., Schweer, T., Peplies, J., Quast, C., Horn, M., et al. (2013).  
700 Evaluation of general 16S ribosomal RNA gene PCR primers for classical and next-  
701 generation sequencing-based diversity studies. *Nucleic Acids Res.* 41, e1.

702 Koenig, A., Zhang, T., Liu, L.-H., and Fang, H. H. P. (2005). Microbial community and  
703 biochemistry process in autosulfurotrophic denitrifying biofilm. *Chemosphere* 58, 1041–  
704 1047.

705 Kuzyk, Z. Z. A., Gobeil, C., Goñi, M. A., and Macdonald, R. W. (2017). Early diagenesis and  
706 trace element accumulation in North American Arctic margin sediments. *Geochimica et  
707 Cosmochimica Acta* 203, 175–200.

708 Kuzyk, Z. Z. A., Gobeil, C., and Macdonald, R. W. (2013).  $^{210}\text{Pb}$  and  $^{137}\text{Cs}$  in margin  
709 sediments of the Arctic Ocean: Controls on boundary scavenging. *Global Biogeochemical  
710 Cycles* 27, 422–439.

711 Kuzyk, Z. Z. A., Macdonald, R. W., and Johannessen, S. C. (2015). Calculating Rates and Dates  
712 and Interpreting Contaminant Profiles in Biomixed Sediments. *Environmental  
713 Contaminants*, 61–87.

714 Laufer, K., Byrne, J. M., Glombitza, C., Schmidt, C., Jørgensen, B. B., and Kappler, A. (2016).  
715 Anaerobic microbial Fe(II) oxidation and Fe(III) reduction in coastal marine sediments  
716 controlled by organic carbon content. *Environ. Microbiol.* 18, 3159–3174.

717 Lavelle, J. W., Massoth, G. J., and Crecelius, E. A. (1985). *Sedimentation Rates in Puget Sound  
718 from  $^{210}\text{PB}$  Measurements*.

719 Lenk, S., Moraru, C., Hahnke, S., Arnds, J., Richter, M., Kube, M., et al. (2012). Roseobacter

720 clade bacteria are abundant in coastal sediments and encode a novel combination of sulfur  
721 oxidation genes. *ISME J.* 6, 2178–2187.

722 Letunic, I., and Bork, P. (2007). Interactive Tree Of Life (iTOL): an online tool for phylogenetic  
723 tree display and annotation. *Bioinformatics* 23, 127–128.

724 Lloyd, K. G., Schreiber, L., Petersen, D. G., Kjeldsen, K. U., Lever, M. A., Steen, A. D., et al.  
725 (2013). Predominant archaea in marine sediments degrade detrital proteins. *Nature* 496,  
726 215–218.

727 Lomstein, B. A., Langerhuus, A. T., D'Hondt, S., Jørgensen, B. B., and Spivack, A. J. (2012).  
728 Endospore abundance, microbial growth and necromass turnover in deep sub-seafloor  
729 sediment. *Nature* 484, 101–104.

730 Marshall, I. P. G., Ren, G., Jaussi, M., Lomstein, B. A., Jørgensen, B. B., Røy, H., et al. (2019).  
731 Environmental filtering determines family-level structure of sulfate-reducing microbial  
732 communities in subsurface marine sediments. *ISME J.*, 1.

733 McMurdie, P. J., and Holmes, S. (2013). phyloseq: An R Package for Reproducible Interactive  
734 Analysis and Graphics of Microbiome Census Data. *PLoS One* 8, e61217.

735 Meire, L., Søgaard, D. H., Mortensen, J., Meysman, F. J. R., Soetaert, K., Arendt, K. E., et al.  
736 (2015). Glacial meltwater and primary production are drivers of strong CO<sub>2</sub> uptake in fjord  
737 and coastal waters adjacent to the Greenland Ice Sheet. *Biogeosciences* 12, 2347–2363.

738 Meyers, P. A. (1994). Preservation of elemental and isotopic source identification of sedimentary  
739 organic matter. *Chemical Geology* 114, 289–302. doi:10.1016/0009-2541(94)90059-0.

740 Müller, A. L., Kjeldsen, K. U., Rattei, T., Pester, M., and Loy, A. (2015). Phylogenetic and  
741 environmental diversity of DsrAB-type dissimilatory (bi)sulfite reductases. *ISME J.* 9,  
742 1152–1165.

743 Müller, A. L., Pelikan, C., de Rezende, J. R., Wasmund, K., Putz, M., Glombitza, C., et al.  
744 (2018). Bacterial interactions during sequential degradation of cyanobacterial necromass in  
745 a sulfidic arctic marine sediment. *Environmental Microbiology* 20, 2927–2940.  
746 doi:10.1111/1462-2920.14297.

747 Mußmann, M., Pjevac, P., Krüger, K., and Dyksma, S. (2017). Genomic repertoire of the  
748 Woeseiaceae/JTB255, cosmopolitan and abundant core members of microbial communities  
749 in marine sediments. *ISME J.* 11, 1276–1281.

750 Nepusz, T., Yu, H., and Paccanaro, A. (2012). Detecting overlapping protein complexes in  
751 protein-protein interaction networks. *Nat. Methods* 9, 471–472.

752 Nobu, M. K., Dodsworth, J. A., Murugapiran, S. K., Rinke, C., Gies, E. A., Webster, G., et al.  
753 (2016). Phylogeny and physiology of candidate phylum “Atribacteria” (OP9/JS1) inferred  
754 from cultivation-independent genomics. *ISME J.* 10, 273–286.

755 Oksanen, J., Blanchet, F. G., Friendly, M., Kindt, R., Legendre, P., McGlinn, D., et al. (2017).  
756 vegan: Community Ecology Package. *Available online at: <http://CRAN.R-project.org/package=vegan>.*

758 Orcutt, B. N., Sylvan, J. B., Knab, N. J., and Edwards, K. J. (2011). Microbial ecology of the  
759 dark ocean above, at, and below the seafloor. *Microbiol. Mol. Biol. Rev.* 75, 361–422.

760 Parks, D. H., Rinke, C., Chuvochina, M., Chaumeil, P.-A., Woodcroft, B. J., Evans, P. N., et al.  
761 (2017). Recovery of nearly 8,000 metagenome-assembled genomes substantially expands  
762 the tree of life. *Nat Microbiol* 2, 1533–1542.

763 Park, S.-J., Park, B.-J., Jung, M.-Y., Kim, S.-J., Chae, J.-C., Roh, Y., et al. (2011). Influence of  
764 deglaciation on microbial communities in marine sediments off the coast of Svalbard,  
765 Arctic Circle. *Microb. Ecol.* 62, 537–548.

766 Pelikan, C., Herbold, C. W., Hausmann, B., Müller, A. L., Pester, M., and Loy, A. (2016).  
767 Diversity analysis of sulfite- and sulfate-reducing microorganisms by multiplex dsrA and  
768 dsrB amplicon sequencing using new primers and mock community-optimized  
769 bioinformatics. *Environ. Microbiol.* 18, 2994–3009.

770 Petro, C., Starnawski, P., Schramm, A., and Kjeldsen, K. U. (2017). Microbial community  
771 assembly in marine sediments. *Aquat. Microb. Ecol.* 79, 177–195.

772 Phillips, E. J. P., and Lovley, D. R. (1987). Determination of Fe(III) and Fe(II) in Oxalate  
773 Extracts of Sediment1. *Soil Science Society of America Journal* 51, 938.  
774 doi:10.2136/sssaj1987.03615995005100040021x.

775 Price, M. N., Dehal, P. S., and Arkin, A. P. (2010). FastTree 2 – Approximately Maximum-  
776 Likelihood Trees for Large Alignments. *PLoS One* 5, e9490.

777 Pruesse, E., Peplies, J., and Glöckner, F. O. (2012). SINA: accurate high-throughput multiple  
778 sequence alignment of ribosomal RNA genes. *Bioinformatics* 28, 1823–1829.

779 Quast, C., Pruesse, E., Yilmaz, P., Gerken, J., Schweer, T., Yarza, P., et al. (2013). The SILVA  
780 ribosomal RNA gene database project: improved data processing and web-based tools.  
781 *Nucleic Acids Res.* 41, D590–6.

782 Ramsey, C. B. (2008). Deposition models for chronological records. *Quaternary Science  
783 Reviews* 27, 42–60.

784 R Core Team (2015). R: The R Project for Statistical Computing. *Available online at:  
785 <http://www.r-project.org/>.*

786 Reimer, P. J., Bard, E., Bayliss, A., Warren Beck, J., Blackwell, P. G., Ramsey, C. B., et al.  
787 (2013). IntCal13 and Marine13 Radiocarbon Age Calibration Curves 0–50,000 Years cal  
788 BP. *Radiocarbon* 55, 1869–1887.

789 Robbins, S. J., Evans, P. N., Parks, D. H., Golding, S. D., and Tyson, G. W. (2016). Genome-  
790 Centric Analysis of Microbial Populations Enriched by Hydraulic Fracture Fluid Additives  
791 in a Coal Bed Methane Production Well. *Front. Microbiol.* 7.  
792 doi:10.3389/fmicb.2016.00731.

793 Schauer, R., Røy, H., Augustin, N., Gennerich, H.-H., Peters, M., Wenzhoefer, F., et al. (2011).  
794 Bacterial sulfur cycling shapes microbial communities in surface sediments of an ultramafic  
795 hydrothermal vent field. *Environ. Microbiol.* 13, 2633–2648.

796 Schloss, P. D., Westcott, S. L., Ryabin, T., Hall, J. R., Hartmann, M., Hollister, E. B., et al.  
797 (2009). Introducing mothur: open-source, platform-independent, community-supported  
798 software for describing and comparing microbial communities. *Appl. Environ. Microbiol.*  
799 75, 7537–7541.

800 Schreiber, L., Holler, T., Knittel, K., Meyer-Dierks, A., and Amann, R. (2010). Identification of  
801 the dominant sulfate-reducing bacterial partner of anaerobic methanotrophs of the ANME-2  
802 clade. *Environ. Microbiol.* 12, 2327–2340.

803 Seidenkrantz, M.-S., Hans Røy, H., Lomstein, B.A., Meire, L. and the shipboard and on-shore  
804 parties, 2014. Godthåbsfjord system and the West Greenland shelf with ‘R/V Sanna’, 11.-  
805 16. August 2013; cruise report. Aarhus University.

806 Shannon, P., Markiel, A., Ozier, O., Baliga, N. S., Wang, J. T., Ramage, D., et al. (2003).  
807 Cytoscape: a software environment for integrated models of biomolecular interaction  
808 networks. *Genome Res.* 13, 2498–2504.

809 Smith, R. W., Bianchi, T. S., Allison, M., Savage, C., and Galy, V. (2015). High rates of organic  
810 carbon burial in fjord sediments globally. *Nature Geoscience* 8, 450–453.

811 Sørensen, H. L., Meire, L., Juul-Pedersen, T., de Stigter, H. C., Meysman, F., Rysgaard, S., et al.  
812 (2015). Seasonal carbon cycling in a Greenlandic fjord: an integrated pelagic and benthic  
813 study. *Mar. Ecol. Prog. Ser.* 539, 1–17.

814 Sørensen, J. (1982). Reduction of ferric iron in anaerobic, marine sediment and interaction with  
815 reduction of nitrate and sulfate. *Appl. Environ. Microbiol.* 43, 319–324.

816 Stamatakis, A. (2014). RAxML version 8: a tool for phylogenetic analysis and post-analysis of  
817 large phylogenies. *Bioinformatics* 30, 1312–1313.

818 Starnawski, P., Bataillon, T., Ettema, T. J. G., Jochum, L. M., Schreiber, L., Chen, X., et al.  
819 (2017). Microbial community assembly and evolution in subseafloor sediment. *Proc. Natl.*  
820 *Acad. Sci. U. S. A.* 114, 2940–2945.

821 Statham, P. J., Skidmore, M., and Tranter, M. (2008). Inputs of glacially derived dissolved and  
822 colloidal iron to the coastal ocean and implications for primary productivity. *Global*  
823 *Biogeochem. Cycles* 22. doi:10.1029/2007gb003106.

824 Stookey, L. L. (1970). Ferrozine---a new spectrophotometric reagent for iron. *Analytical*

825 *Chemistry* 42, 779–781. doi:10.1021/ac60289a016.

826 Svendsen, H., Beszczynska-Møller, A., Hagen, J. O., Lefauconnier, B., Tverberg, V., Gerland,  
827 S., et al. (2002). The physical environment of Kongsfjorden–Krossfjorden, an Arctic fjord  
828 system in Svalbard. *Polar Res.* 21, 133–166.

829 Teske, A., Durbin, A., Ziervogel, K., Cox, C., and Arnosti, C. (2011). Microbial community  
830 composition and function in permanently cold seawater and sediments from an arctic fjord  
831 of svalbard. *Appl. Environ. Microbiol.* 77, 2008–2018.

832 Thamdrup, B., Fossing, H., and Jørgensen, B. B. (1994). Manganese, iron and sulfur cycling in a  
833 coastal marine sediment, Aarhus bay, Denmark. *Geochim. Cosmochim. Acta* 58, 5115–  
834 5129.

835 Thrash, J. C., Cameron Thrash, J., Seitz, K. W., Baker, B. J., Temperton, B., Gillies, L. E., et al.  
836 (2017). Metabolic Roles of Uncultivated Bacterioplankton Lineages in the Northern Gulf of  
837 Mexico “Dead Zone.” *MBio* 8, e01017–17.

838 Trembath-Reichert, E., Case, D. H., and Orphan, V. J. (2016). Characterization of microbial  
839 associations with methanotrophic archaea and sulfate-reducing bacteria through statistical  
840 comparison of nested Magneto-FISH enrichments. *PeerJ* 4, e1913.

841 Wang, Q., Garrity, G. M., Tiedje, J. M., and Cole, J. R. (2007). Naive Bayesian classifier for  
842 rapid assignment of rRNA sequences into the new bacterial taxonomy. *Appl. Environ.*  
843 *Microbiol.* 73, 5261–5267.

844 Wang, Y., Gao, Z.-M., Li, J.-T., Bougouffa, S., Tian, R. M., Bajic, V. B., et al. (2016). Draft  
845 genome of an Aerophobetes bacterium reveals a facultative lifestyle in deep-sea anaerobic  
846 sediments. *Sci Bull. Fac. Agric. Kyushu Univ.* 61, 1176–1186.

847 Wasmund, K., Schreiber, L., Lloyd, K. G., Petersen, D. G., Schramm, A., Stepanauskas, R., et al.  
848 (2014). Genome sequencing of a single cell of the widely distributed marine subsurface  
849 Dehalococcoidia, phylum Chloroflexi. *ISME J.* 8, 383–397.

850 Wasmund, K., Cooper, M., Schreiber, L., Lloyd, K. G., Baker, B. J., Petersen, D. G., et al.  
851 (2016). Single-Cell Genome and Group-Specific dsrAB Sequencing Implicate Marine  
852 Members of the Class Dehalococcoidia (Phylum Chloroflexi) in Sulfur Cycling. *MBio* 7,  
853 doi:10.1128/mbio.00266-16.

854 Wasmund, K., Mußmann, M., and Loy, A. (2017). The life sulfuric: microbial ecology of sulfur  
855 cycling in marine sediments. *Environ. Microbiol. Rep.* 9, 323–344.

856 Webster, G., Sass, H., Cragg, B. A., Gorra, R., Knab, N. J., Green, C. J., et al. (2011).  
857 Enrichment and cultivation of prokaryotes associated with the sulphate-methane transition  
858 zone of diffusion-controlled sediments of Aarhus Bay, Denmark, under heterotrophic  
859 conditions. *FEMS Microbiol. Ecol.* 77, 248–263.

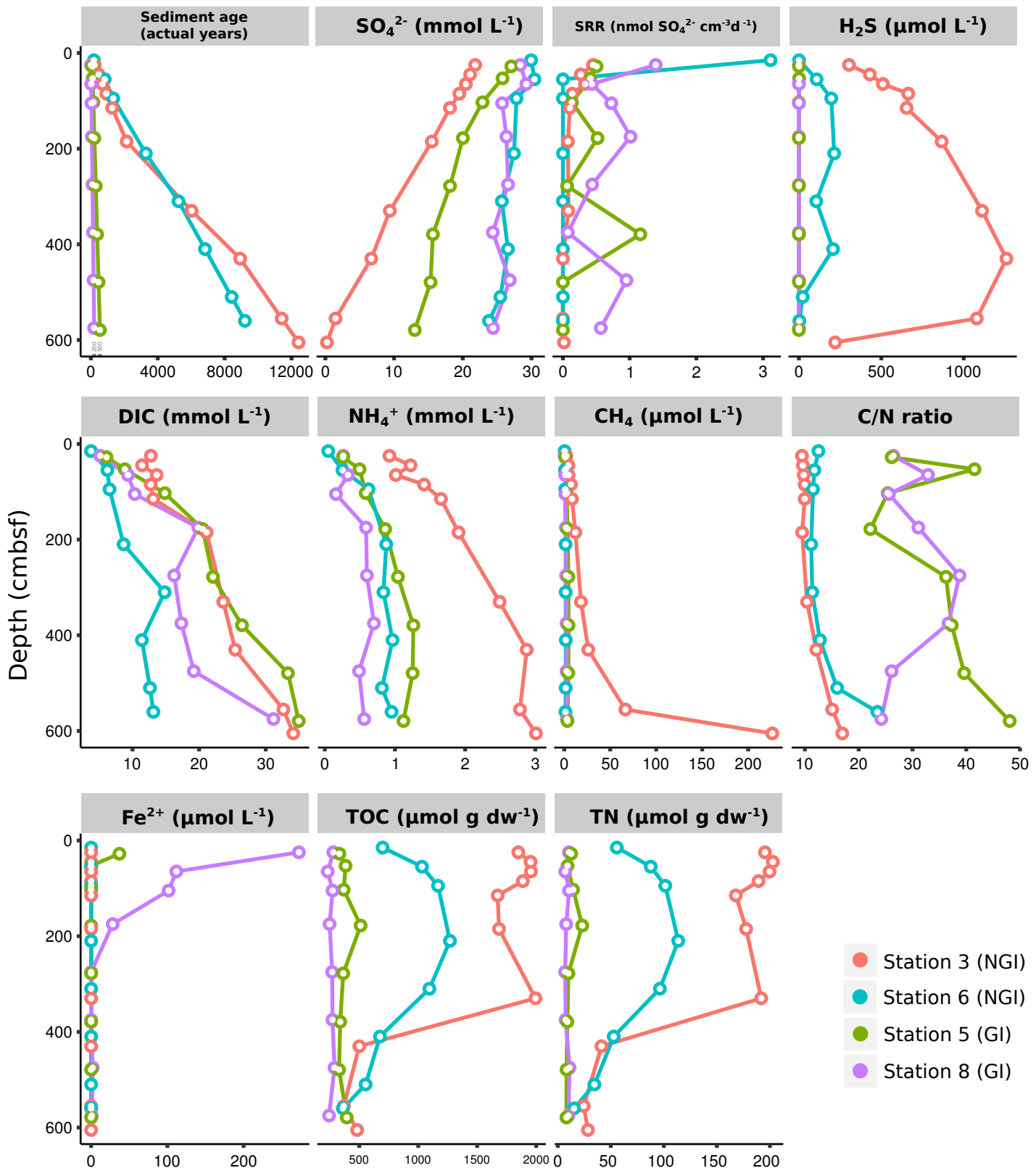
860 Wehrmann, L. M., Formolo, M. J., Owens, J. D., Raiswell, R., Ferdelman, T. G., Riedinger, N.,  
861 et al. (2014). Iron and manganese speciation and cycling in glacially influenced high-  
862 latitude fjord sediments (West Spitsbergen, Svalbard): Evidence for a benthic recycling-  
863 transport mechanism. *Geochim. Cosmochim. Acta* 141, 628–655.

864 Wehrmann, L. M., Riedinger, N., Brunner, B., Kamyshny, A., Hubert, C. R. J., Herbert, L. C., et  
865 al. (2017). Iron-controlled oxidative sulfur cycling recorded in the distribution and isotopic  
866 composition of sulfur species in glacially influenced fjord sediments of west Svalbard.  
867 *Chem. Geol.* 466, 678–695.

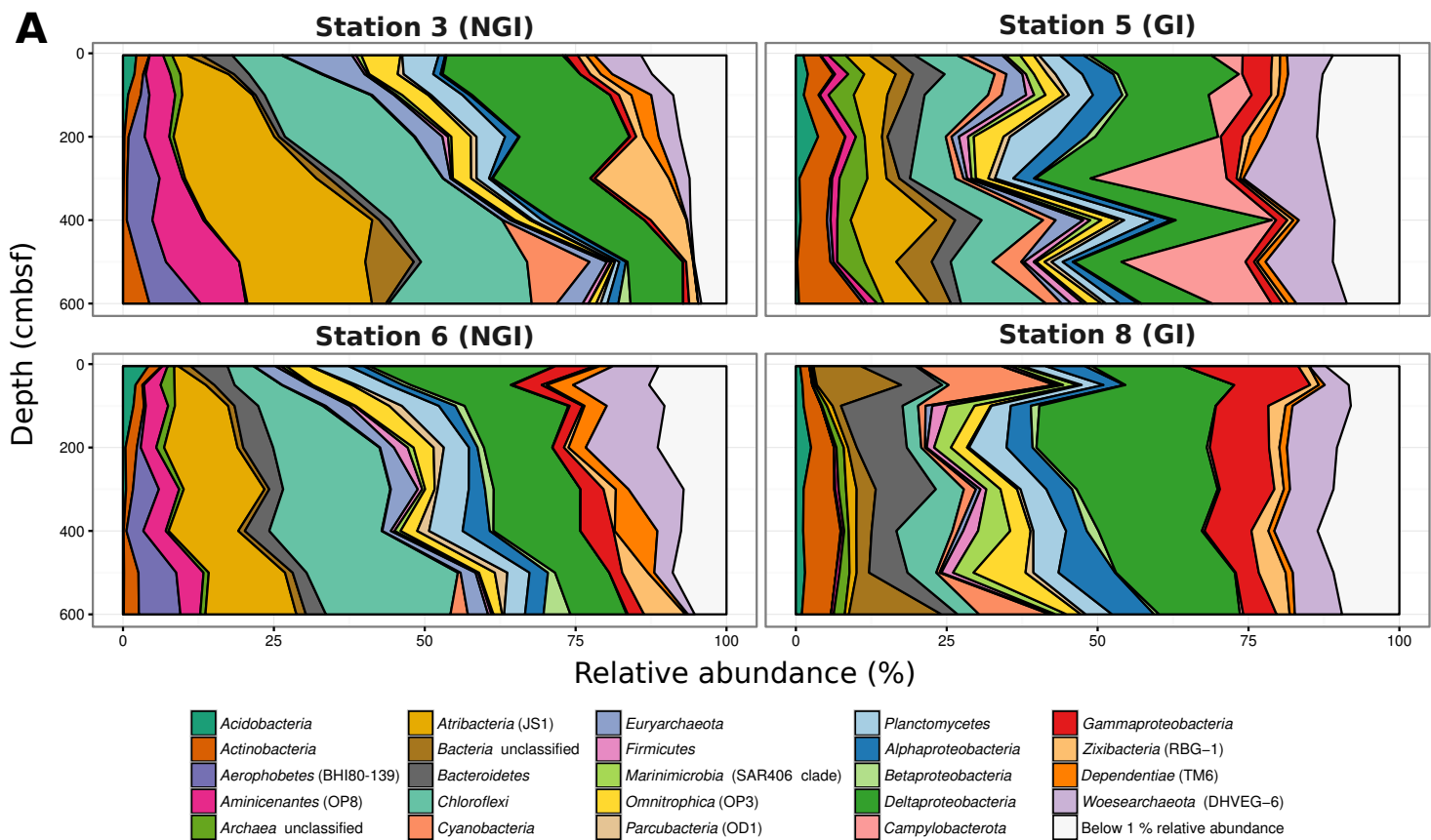
868 Weiss, S., Van Treuren, W., Lozupone, C., Faust, K., Friedman, J., Deng, Y., et al. (2016).  
869 Correlation detection strategies in microbial data sets vary widely in sensitivity and  
870 precision. *ISME J.* 10, 1669–1681.

871 Zajączkowski, M. (2008). Sediment supply and fluxes in glacial and outwash fjords,  
872 Kongsfjorden and Adventfjorden, Svalbard. *Polish Polar Research* 29, 59–72.

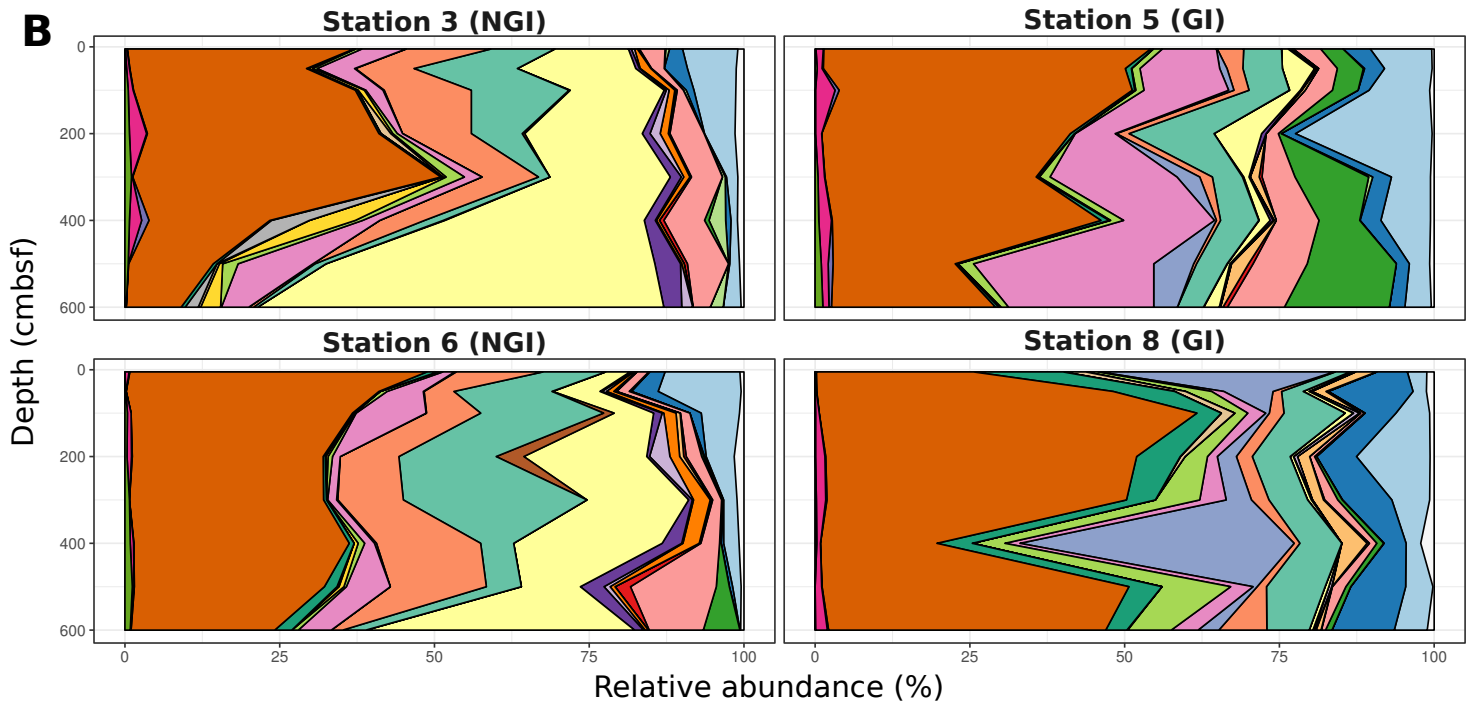
873 Zopfi, J., Ferdelman, T. G., and Fossing, H. (2004). “Distribution and fate of sulfur  
874 intermediates—sulfite, tetrathionate, thiosulfate, and elemental sulfur—in marine  
875 sediments,” in *Special Paper 379: Sulfur Biogeochemistry - Past and Present*, 97–116.



**A**



**B**

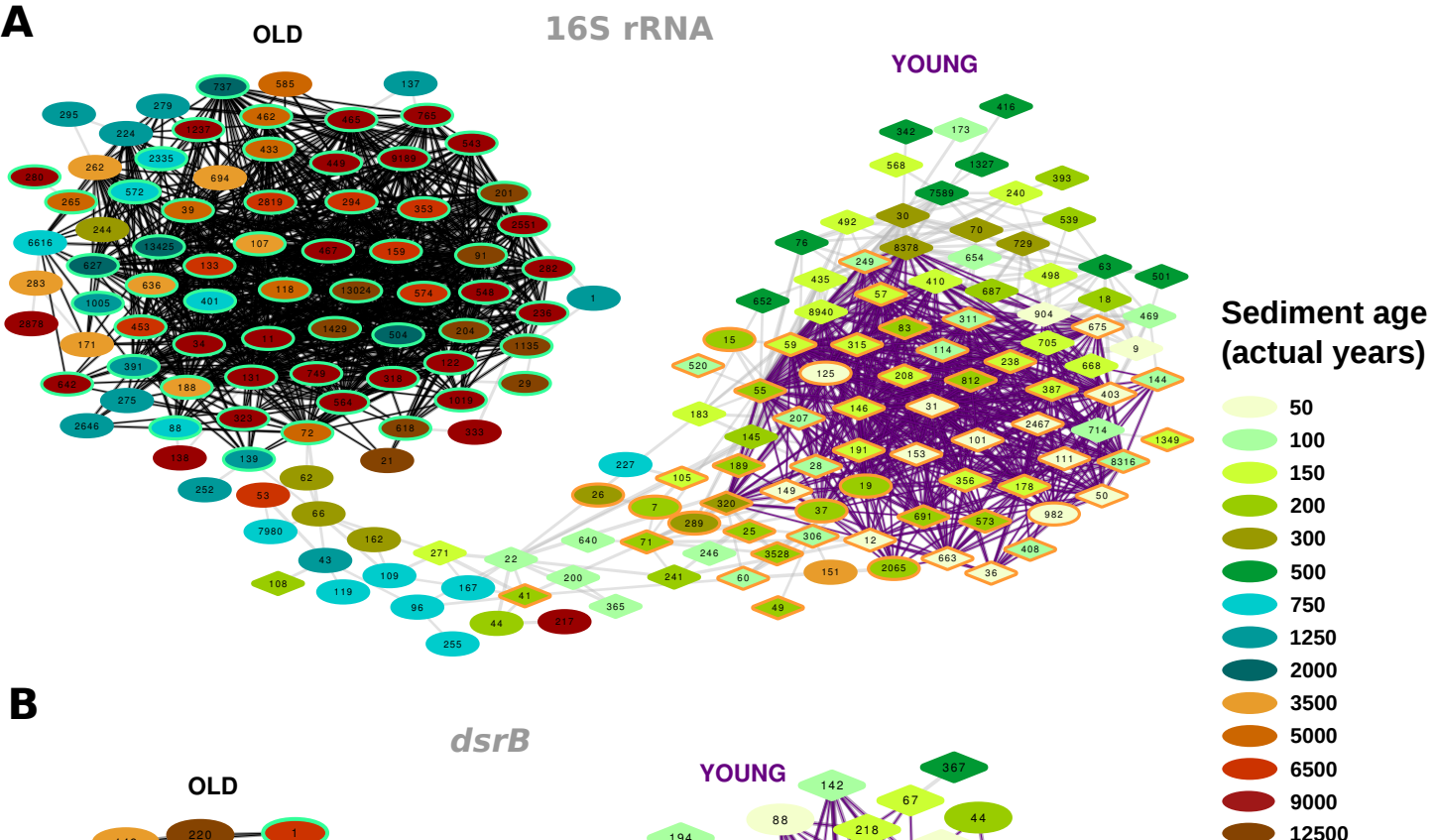


Desulfatiglans anilini lineage  
Desulfoarculus baarsii lineage  
Desullobacca acetoxidans  
Desulfobacteraceae  
Desulfovulbaceae  
Desulfohalobiaceae  
Desulomonile tiedjei lineage  
Desulfovibrionaceae  
ES1 - unclassified

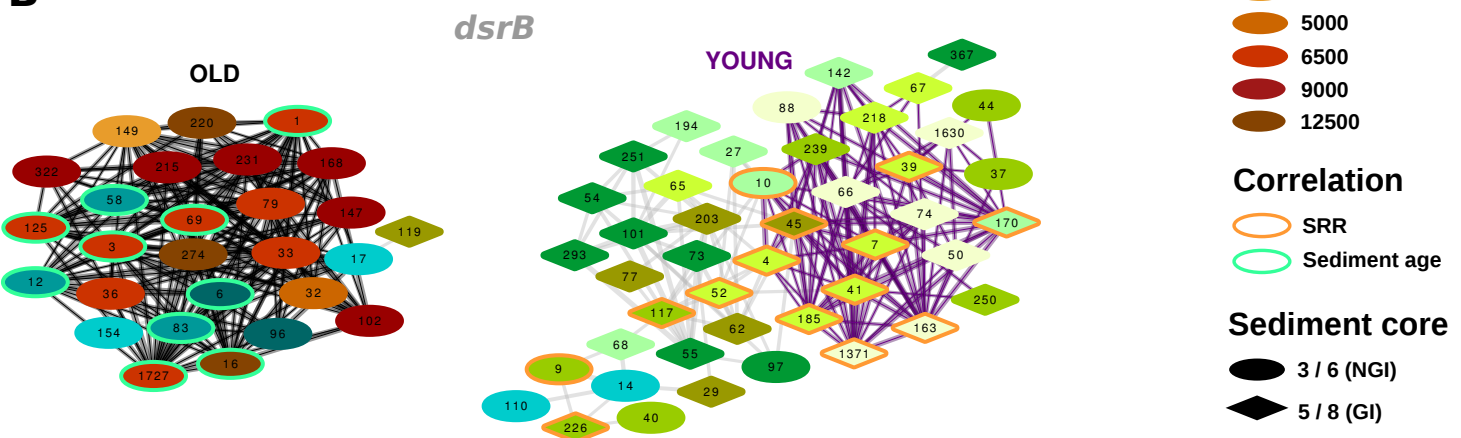
FG - unclassified  
Nitrospirae supercluster unclassified  
Syntrophobacteraceae  
Uncultured bacteria (incl. bins from multiple phyla/classe) - ES1  
Uncultured bacteria (incl. Chloroflexi SAG DEH-C11) - FG  
Uncultured bacteria (incl. Deltaproteobacteria RBG 13 43 22) - DS  
Uncultured bacteria (incl. Deltaproteobacteria RBG 13 61 14) - FG  
Uncultured DsrAB family-level lineage 1  
Uncultured DsrAB family-level lineage 12

Uncultured DsrAB family-level lineage 13 (incl. *Thermodesulfovibrionia*)  
Uncultured DsrAB family-level lineage 2  
Uncultured DsrAB family-level lineage 3  
Uncultured DsrAB family-level lineage 4  
Uncultured DsrAB family-level lineage 5 (incl. novel metagenome bins)  
Uncultured DsrAB family-level lineage 7  
Uncultured DsrAB family-level lineage 9 (incl. Acidobacteria)  
Below 1 % relative abundance

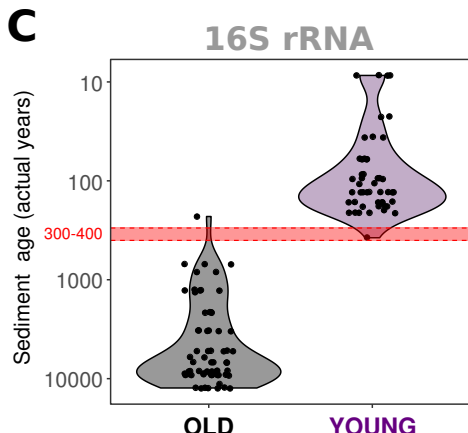
**A**



**B**



**C**



**D**

